Journal of Science and Engineering Technology, Vol. 2, No. 3, pp. 9-20 (2006)

An Experimental Investigation of the Turbulence Structure of a Block-Mounted Rectangular Channel Flow

KUN-CHIEH WANG[1] and WEN-RUEY CHEN[2]
[1]*Department of Information Management, Ling Tung University*
1 Ling Tung Rd., Nantun, Taichung, Taiwan
[2]*Formosa Plastics Group*
100 Swei Kuan Rd., Jen-Wu, Kaohsiung, Taiwan

ABSTRACT

This study examines in detail the turbulence structure in a fully-developed turbulent channel flow with a block mounted on one principal wall via laser-Doppler velocimetry (LDV) at Re=1.15×10^4, BR=0.5, and W / H=2. The variations in major fluctuating parameters throughout the flow, including the axial mean velocity, turbulence intensity, turbulent kinetic energy and Reynolds stress, are examined. A refractive-index-matched fluid is adopted during the test to permit access to the near-wall region without distorting the laser beam. The experimental results indicate that four circulating bubbles exist around the block, thereby characterizing the flow structure. The largest circulating bubble is located behind the block (the main recirculation region); the bubble begins at the trailing edge of the block and reattaches itself onto the bottom wall of the channel with a reattachment length of 6.6H. In the main recirculation region, the axial mean velocity distributions do not obey the log-law. However, the viscous-sublayer linear relationship $U^+=Y^+$ is maintained when the fluid is sufficiently near the channel wall. After departing from the reattachment point, the axial mean velocity of the fluid gradually approaches the log-law distribution while in the near-wall region. In the main recirculation region, there is a strong correlation between C_{fN} and Re_N, where C_{fN} varies in the range of 0.01~0.04, being higher than that in a normal turbulent boundary layer. The axial turbulence intensity of the fluid is distributed differently around the block. This implies that the assumption of isotropic flow in the analysis of the turbulent flow over a protruding block(s), although widely used in numerical computations for turbulent flows, is no longer suitable. The global maximums for turbulence intensity, turbulent kinetic energy, and Reynolds stress all occur in the top region of the block at stations about X / H=0.5~1.2; the second maximums for these parameters all appear at stations about 2~3H before the main reattachment point.

Key Words**:** turbulence structure, block-mounted channel flow, LDV measurement, circulating bubble, refractive-index-matched method

具凸塊障礙物之矩形渠道紊流結構之實驗探討

王焜潔[1]　陳文瑞[2]
[1]嶺東科技大學資訊管理學系
台中市南屯區嶺東路 1 號
[2]台塑重工
高雄縣仁武鄉水管路 100 號

摘 要

本文利用雷射都卜勒測速儀研究具凸塊障礙物之完全擴展渠道流在 Re=11500，BR=0.5，及 W/H=2 狀況下之紊流結構。相關流場結構之主要擾動參數包括軸向平均速度、紊流強度、紊流動能及雷諾剪應力等均詳加探討。本研究採用折射率配合之流體以使近壁處之雷射光束不致扭曲。實驗結果顯示共有四個特徵迴流包出現在凸塊四周。最大迴流包出現在凸塊後方之主迴流區，此迴流包始於凸塊後緣，附著於渠道底板上，附著長度爲 6.6H。主迴流區內軸向平均速度不遵循對數律之速度分佈；然而在近壁之層流次層區域，$U^+=Y^+$ 之關係仍然成立。附著點之後，近壁流體之軸向平均速度漸趨向對數律之速度分佈。在主迴流區內，摩擦係數 C_{fN} 與雷諾術數 Re_N 有強烈相關性；C_{fN} 在 0.01~0.04 之間變化，較一般完全擴展紊流之邊界層者大。另一方面，軸向紊流強度之分佈在凸塊周圍差異甚大；此意味著常於紊流數值計算上所假設之紊流等向性用之於本研究或類似之流場並不適當。全域之紊流強度、流動能及雷諾剪應力之極大值發生於凸塊頂部約 X/H=0.5~1.2 之截面；而次極大值則發生於主迴流區附著點前約 2~3H 之位置。

關鍵詞：紊流結構，具凸塊障礙物之渠道流，雷射都卜勒測速儀，迴流包，折射率配合法

I. INTRODUCTION

Ribs are commonly used in internal duct flows to promote the heat transfer from the surface by providing a greater surface area for heat transfer and by periodically interrupting the wall boundary layer causing flow separation, circulation, and reattachment. The industrial applications of particular interest include high-temperature gas-cooled nuclear reactors, turbine vane end-wall cascade temperature, and heat transfer coefficient distributions, flow blockages in heat exchangers, and electronic equipments. There are numerous experimental publications in which the effectiveness of the aforementioned augmentation was investigated. Flow visualizations conducted by Durst and Rastogi [9] revealed that the length of the downstream recirculation bubble varies in the range of about 5~16 rib heights, depending on the rib shape and degree of the flow blockage caused by the ribs. Bergeles and Athanassiadis [3] and Antoniou and Bergeles [2] used a single-wire anemometer to study the flow past a two-dimensional rib. Liou and Kao [15] performed the laser-Doppler measurements behind blocks and found that the peak turbulence intensity occurred within the downstream recirculation region at about 1.5 rib heights upstream of reattachment. Ratts et al. [21] presented an experimental study of internal flow modulation induced by vortex shedding from cylinders in cross-flow and its effect on cooling of an array of chips. Myrum et al. [18] investigated the heat transfer and the pressure characteristics of airflow in a ribbed duct with vortex generator placed immediately upstream or just downstream of selected rib elements. Provided the diameter of the generator is large, the average Nusselt number was increased by as much as 21%. Jurbran et al. [13] reported experimental investigations into the effect of rectangular and non-cubic obstacles of various lengths, widths, and heights on pressure drop and heat transfer enhancement. It was found that changes in obstacle size or shape can lead to Nusselt number increases as high as 40%. Chen and Wang [6] examined the forced convective flow over two sequentially heated blocks mounted on one principal wall of an horizontal channel, and they found that the reattachment of the separating bubble and the flow impingement significantly influence the heat transfer from the channel surface. Olsson and Sundén [19] experimentally investigated the secondary flow patterns, pressure drop, and heat transfer in rib-roughened rectangular channels with different rib geometries and aspect ratios. Buchlin [4] revealed that, for different types of turbulator, the increase of the open-area ratio of the perforated rib up to 36% and for Reynolds number based on the obstacle height higher than 2×10^4, significantly improves the heat exchange. Meinders and Hanjalic [17] experimentally studied the convective heat transfer from in-line and staggered configurations of two wall-mounted cubes, and they found that flow reattachment caused typically a monotonic decay of the convective heat transfer and, on the contrary, flow separation caused distinct heat transfer extremes at the cube faces.

From the above literature survey, it is known that most of the published works were focusing on the flow structure away from the wall. However, close to the wall, questions regarding the turbulence properties still remain, since the experimental results are inconsistent and in some details contradict the results obtained from direct numerical

simulations [10, 14, 16]. These evidences suggest that more refined experimental works are needed in the near-wall region of turbulent boundary layers, pipe and channel flows. Due to the small thickness of the viscous sublayer, most measurement techniques used so far failed to satisfy the space and/or time resolution requirements imposed by the flow structure. This gives birth to so called "refractive-index-matched method". Traditionally, measurements in viscous sublayer of liquid flows using LDV require a well-designed test rig to avoid deflections of light beams near the solid surface. It is obviously tedious and time-consuming. To overcome this weakness, the use of refractive-index-matched fluids can effectively eliminate influences of the channel walls on the laser beams.

The objective of this paper aims to measure U, C_f, U', V', K, and τ_t by LDV in conjunction with the method of refractive-index matching in order to investigate the near-wall turbulence structure of a turbulent block-mounted rectangular channel flow.

II. TEST SECTION AND INSTRUMENTATION

1. Testing Loop

Sketches of the testing loop are given in Fig. 1. The working fluid was drawn from an oil tank into the test section through a filter and a flow straightener (with a length of *350 cm* to ensure a fully-developed flow condition at the inlet of test section) and a 4-to-1 contraction by an oil pump. The flow straightener was made by acryl resin with size of 20*cm*(length)×10*cm*(width)×8*cm*(height). The test fluid then flowed through the mounted block, a divergent-convergent section, and went back to the oil tank. In order to permit laser-Doppler measurements, the test section was made from a highly homogeneous acryl resin duct. To avoid any interference of the duct with the light beams, the test fluid was selected to be refractive-index-matched to the acryl resin, the material of the duct wall. To achieve precise matching of refractive indices, two liquid oils of slightly different refractive indices were selected and carefully mixed. One of the liquid oils is turpentine, about 68.2% by volume and the other is tetraline, about 31.8% by volume. The resulting properties at 29±1°*C* are $\rho = 894 kg/m^3$ and $\nu = 1.589\times10^{-6} m^2$/sec. In addition, the heating and cooling elements installed in the downstream settling chamber of the test rig controlled the temperature of the test fluid. In this way, the temperature controller permits thermal effects on the refractive index of the test fluid to be kept within $\pm5\times10^{-4}$. This was found to be sufficient to ensure undisturbed velocity measurements close to the duct walls.

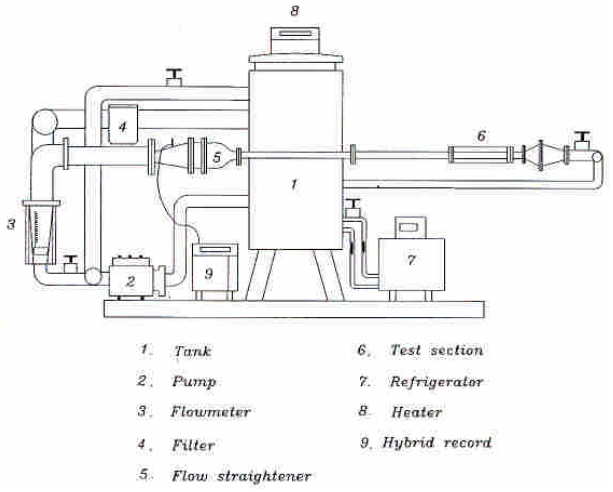

Fig. 1. The closed-type testing loop

2. Instrumentation

A special laser-Doppler optical system was designed for the present measurement. This system is schematically shown in Fig. 2. The system operates with a 2W argon-ion laser and double Bragg cell transmission optics. The LDV optics was set up in a dual beam forward scattering configuration. This Laser beam was split into two parallel beams of equal intensity by a beam-splitter. A Bragg cell was used to cause a 40-*MHz* frequency shift on the beams. The frequency shift is used to eliminate the direction ambiguity, which is essential if there is flow reversal. The resulting pair of beams was then passed through a focal lens, entered the test section through the glass wall, intersected inside the duct, and gave a probe volume with dimensions of 0.52*mm* by 0.097*mm*, and then passed through another glass wall into the beam traps. The entire LDV system was mounted on a milling machine with four vibration isolation mounts. The laser light scattered from the seeding particles was collected by a receiving optical package and a photomultiplier. The detected signal was electrically down-mixed to the appropriate frequency shift. Then, a counter processor with 2 *ns* resolutions was used to process the Doppler signal. The seeding particles were introduced into the liquid stream by four atomizers.

3. Test conditions

The test duct was made from a 4 *cm* thick acryl resin and had a cross-section of 20*cm*(*width*)×2*cm*(*height*). The block's width-to-height ratio *W/H* and the blockage ratio *BR* were chosen as 2 and 0.5, respectively. In the testing case of smooth-duct flows, the Reynolds number was kept at 1.15×10^4 and the free stream intensity was restricted under 4%. The velocity measurements were carried out at various stations

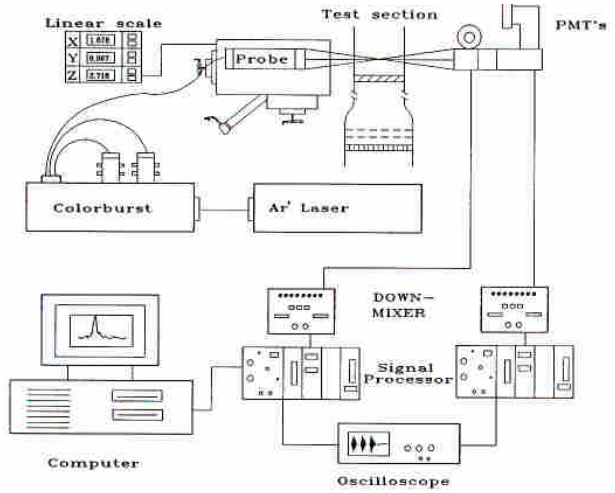

Fig. 2. Fiber-optic LDV system

along the centerline plane of the duct at Z/W_c=1/2. For every measuring run, a total of 44 profiles and 37 points for each profile were taken. A rotating disk with known constant speed corrected the LDV system and the deviation of measured velocity was found within 0.15%. The uncertainties occurred in the LDV measurements include statistical and instrumental uncertainties. Followings are the estimated uncertainties in experiment: 0.5% for the axial velocity, 0.32% for the transverse velocity, 0.61% for the axial turbulence intensity, 0.61% for the transverse turbulence intensity, 0.7% for the Reynolds stress and turbulent kinetic energy, and 0.55% for the Reynolds number within 95% confidence level.

Two different types of channel flows were under consideration. Firstly, the turbulent flow in a smooth rectangular channel without blocks is considered. This case is concerned primarily to test the validity of the measurement apparatus and technique used in our study. Secondly, the turbulent rectangular channel flow with a mounted block is studied. This case is the major target of our study. All turbulent crucial fluctuating parameters regarding the flow structure throughout the flow will be measured and discussed, especially in the near-wall recirculation region.

III. RESULTS AND DISCUSSIONS

1. Flow in a smooth channel

Distribution measurements of the axial mean velocity, axial turbulence intensity, turbulent kinetic energy, and Reynolds stress along a smooth channel were taken at Re=1.15×10^4 and *AR*=10 in order to test the uniformity, repetivity, and the fully developed characteristics of flows. Experimental results of the distribution of axial mean velocity in the spanwise direction, measured at the station *X/H*=-8 and *Y/H*=1, show good two-dimensional uniformity. Additionally, measurement results of the axial mean velocity distribution in the streamwise direction identify that the deviation between two peak values of the axial mean velocity at *X/H*=-8 and *X/H*=-10 is estimated about 0.1%. This finding means that the flow was already fully developed before reaching the block. The measured entrance length of flow is about 1*m*. The deviation of maximal axial mean velocities measured at station *X/H*=-8 on different days is estimated at less than 0.2%. In the near-wall region, distribution results for axial fluctuation velocity, turbulent kinetic energy, and Reynolds stress, given in Fig. 3, demonstrate that these measured data approach to those obtained by Jonansson and Alfredsson [12]. Besides, according to the foundings by Patel et al. [20] and Coles [7], for their investigations in a smooth fully developed rectangular channel flow, the distributions of measured axial fluctuation velocity, turbulent kinetic energy, and Reynolds stress are scattering in the range of ±25% to our data. This confirms the validation of our measurement results. Furthermore, the measured axial mean velocity distribution in the near-wall region at station *X/H*=-8 coincides well with the results obtained by theoretical log-law predictions, as shown in Fig. 4.

Generally, experimental data for axial turbulence intensity, turbulent kinetic energy, and Reynolds stress in this work are in agreement with previously published data. The encouraging ability of the present procedures to predict turbulent fluctuating characteristics in a smooth channel flow lends strong support to the evaluation of the block-roughened channel flow in the following study.

2. Flow past a wall-mounted block

A. Flow structure

In a channel flow with wall-mounted blocks, phenomena

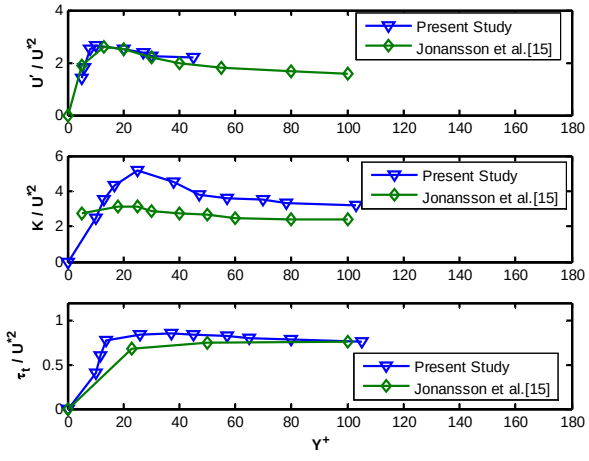

Fig. 3. Near-wall variations of flow parameters in a smooth channel flow

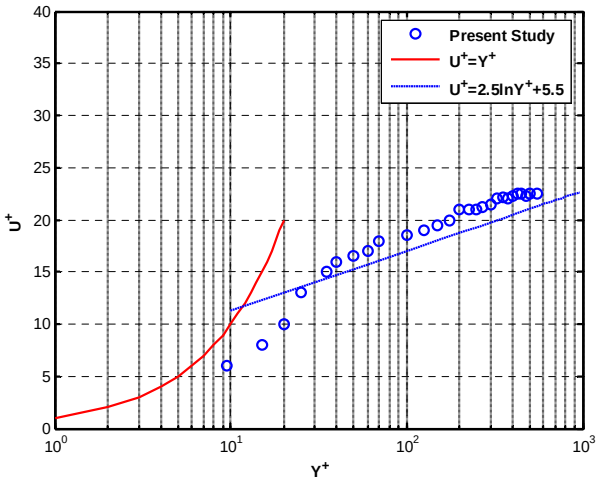

Fig. 4. Comparison of axial mean velocities

of the boundary layer separation, recirculation, reattachment, and redevelopment frequently occur in the flow field. In this study, four separating bubbles were found around the block. Figure 5 shows a typical case of configuration of the mean velocity vector at Re=11500, *BR*=0.5, and *W/H*=2. The first small circulating bubble occurs in front of the block,near the bottom wall of the channel. The second circulating bubble occurs upon the block, starting at the leading edge of the block and is attached to the block's top surface. The third bubble, the largest separating bubble in the main recirculation region, occurs behind the block. This bubble is produced by a significant reduction in fluid momentum and strong adverse pressure gradient caused by area-expansion. The last bubble, a small separating bubble, is located inside the main recirculation region and is just attached to the bottom-rear corner of the block. The lengths of these four separating bubbles can be obtained from the schematic of the streamline patterns derived from the axial and transverse mean velocity distributions in the flow field. Table 1 summarizes these results. Observations show that the reattachment length of the main recirculation region is generally about 6.6 times the block height. This reattachment length is approximately the same magnitude as that found in a backward stepping flow [23].

B. Axial mean velocity distribution

Figure 6 shows the axial mean velocity distribution along the channel. This velocity illustrates the time-averaged behavior of flow structures. The flow around the block is divided into three regions: front, above, and rear. (1) In the front region of the block, the axial mean velocity is fully developed with a maximum value as high as 0.4 m/sec at X/H=-8. Next, the axial mean velocity gradually decreases along the channel. Near the front face of the block, an area

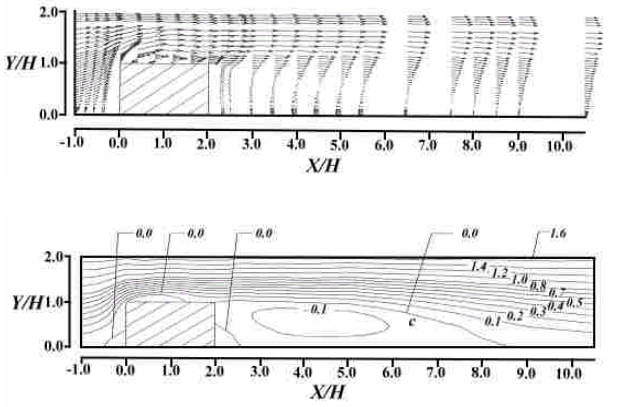

Fig. 5. Configurations of the mean velocity vector and streamline pattern

Table 1. Reattachment lengths of separating bubbles

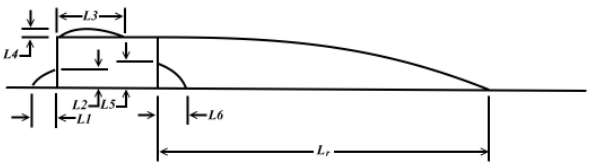

L1	L2	L3	L4	L5	L6	L_r
0.47H	0.28H	1.34H	0.16H	0.52H	0.61H	6.6H

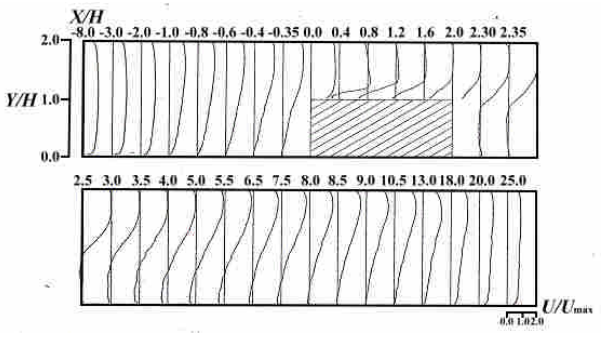

Fig. 6. Axial mean velocity distributions

with negative axial mean velocity develops which indicates the existence of a recirculation region. (2) In the upper region of the block, the cross-sectional maximal axial mean velocities at stations X/H=0.4, 0.8, 1.2, and 1.6, are at least two times larger than that at station X/H=-8. The explanation for this phenomenon is that the effect of area-contraction above the block accelerates the fluid motion and at the same time causes flow separation near the upper face of the block. (3) In the rear region of the block, the cross-sectional peak value of axial mean velocity gradually declines in streamwise direction.

Specifically, a clear zero-velocity line occurs, i.e., a separation line that runs from the trailing edge of the block to the stagnation point at the bottom wall of the channel. Flow fluctuation near this separation line is significantly larger than anywhere else. This separation line divides the flow into the main flow (above the separation line) and the circulating flow (below the separation line). A large negative-velocity area in the flow under the separation line confirms the existence of a significantly large recirculation region. In the flow above the separation line, the main stream gradually expands and decelerates as it moves toward the channel outlet. Axial mean velocity distributions in such a main recirculation region are essential to an analysis of the structure of turbulent separating flows. Usually, it is used as a performance index in turbulence modeling calculation as well as a challenge in measurement techniques. As $X/H \geq 25$, the axial mean velocity distribution returns to a fully-developed condition, similar as that at X/H=-8.

C. Near-wall axial mean velocity distribution in the main recirculation region

It has already been demonstrated that, in the turbulent smooth channel flow, the measured near-wall axial mean velocity follows the log-law distribution. Figure 7 shows the measured near-wall axial mean velocity distributions before and after the reattachment point in the main recirculation region. Before the reattachment point (Fig. 7(a)), the near-wall axial mean velocity closely matches the line $U^+=-Y^+$ as $Y^+ \leq 10$. However, this axial mean velocity has a large discrepancy from the log-law distribution of $U^+ = 2.5\ln Y^+ + 5.5$ as $Y^+ > 10$. This phenomenon reveals that the near-wall turbulent structure in the main recirculation region is quite different from that in a fully developed turbulent boundary layer. After the reattachment point (Fig. 7(b)), (1) as $Y^+ \leq 10$, the axial mean velocity distributions closely match the equation $U^+=Y^+$; but, (2) as $Y^+>10$, the axial mean velocity distributions gradually vary toward $U^+ = 2.5\ln Y^+ + 5.5$ in the streamwise direction. This phenomenon suggests a considerably change occurs in the turbulent boundary layer transforming from separation-dominated structure towards fully developed structure. A similar finding was reported by Simpson, Chew and Shivaprasad [23] in their study of the recirculation region which was noted to be a result of the pressure gradient in flows around an airfoil.

D. Skin-friction coefficient

Skin friction coefficient is an important parameter characterizing the flow structure, especially in the recirculation region for various turbulent flow conditions. To understand its variations, this work first compares the distribution of

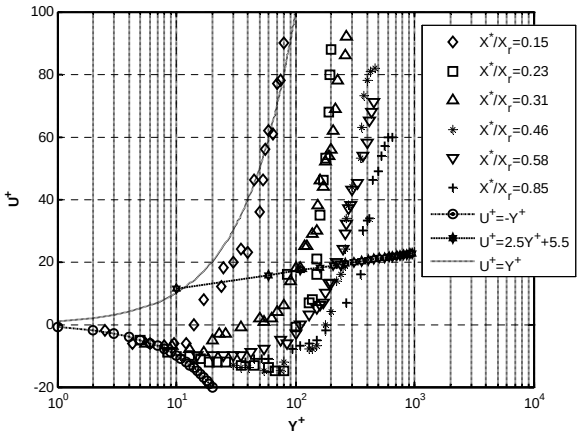

(a) U^+ before the reattachment point

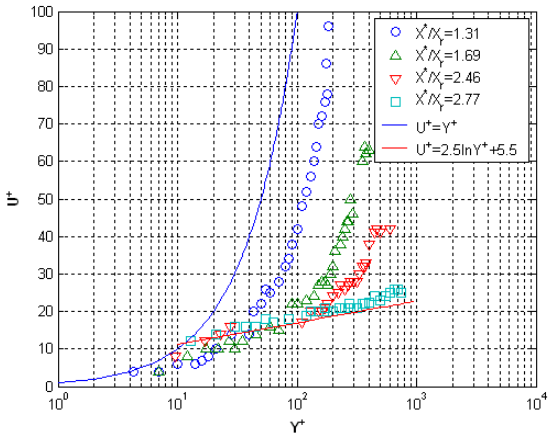

(b) U^+ after the reattachment point

Fig. 7. Near-wall axial mean velocity distributions in the main recirculation region

skin-friction coefficients at different downstream locations in the main recirculation region behind the block with those presented in Ruderich and Fernholz [22] and Castro and Haque [5] in which, respectively, flows through a splitter plate and a backward-facing step in the downstream recirculation region were considered. As shown in Fig. 8, similar distributions of C_f around the reattachment were found. This finding indicates that substantially similar turbulence structures exist in all three studies. Furthermore, Fig. 8 shows that the skin-friction coefficient (C_f) changes from positive to negative at X^*/X_r=0.055 and from negative to positive at X^*/X_r=0.8, indicating that a different near-wall flow pattern between exists between these two points. At X^*/X_r=1, i.e., the stagnation point, C_f becomes 0. This result is produced by the effect of a zero-velocity gradient at the stagnation point. After the reattachment point, the skin-friction coefficients gradually approach to a constant value. This finding is coincident with findings by Runderich and Fernholz [22] who noted that, far

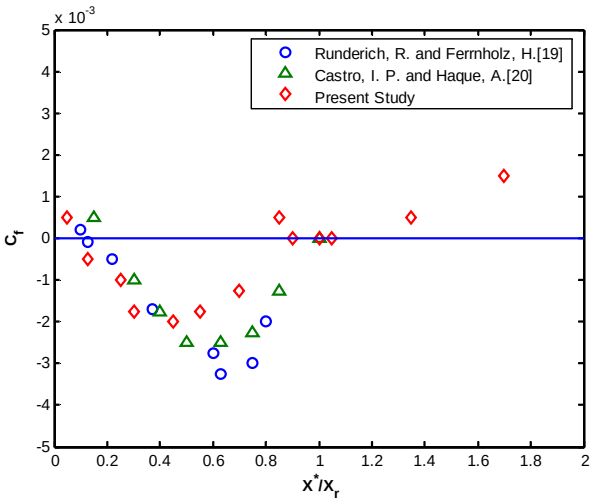

Fig. 8. Skin friction coefficient variations in the main recirculation region

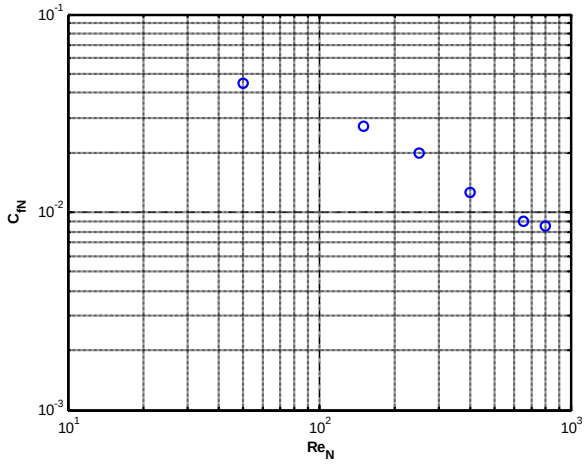

Fig. 9. Skin friction coefficient versus wall-shear-layer Reynolds number

behind the stagnation point, the skin-friction coefficient remains unchanged at a fixed Reynolds number. Moreover, it is worth noting that another essential definition exists for the skin-friction coefficient: $C_{fN}=2\tau_w/\rho U_N^2$ (Adams and Johnston [1]). Fig. 9 presents the variation of this new defined skin-friction coefficient (C_{fN}) with shear-layer Reynolds number Re_N. There is a strong correlation between C_{fN} and Re and C_{fN} has a slope of about -1/2, which is in agreement with the findings in Adams and Johnston [1] and Driver and Seegmiller [8]. In the main recirculation region, the skin-friction coefficient $|C_{fN}|$ varies in the range of 0.01~0.04 for different Reynolds numbers, which is a variation range significantly large than the level of those found in fully developed turbulent boundary layer flows. This finding illustrates that the turbulent flow structure in the near-wall recirculation region deviates dramatically from that in the fully developed turbulent boundary layer. This phenomenon is generally regarded as a laminar-like structure: it is not true laminar boundary layer structure since substantial fluctuations still exist.

E. Turbulence intensity

Ribs are often used as turbulence promoters to enhance heat transfer. Moreover, heat transfer is strongly dependent on turbulence intensity. Han et al. [11] examined a case of heat transfer enhancement in channels with turbulence promoters - similar to that examined in this study- and determined that extremely high heat transfer coefficients as well as turbulence intensities occurred at the leading edge of the rib and the reattachment point behind the rib. Low heat transfer coefficients were found on the rear surface of the rib. Since the strength of turbulence intensity has a dramatic influence on the heat transfer from blocks, detailed investigations of the turbulence intensity are critical. Figures 10 and 11 indicate that both axial and transverse turbulence intensities have similar profiles along the channel. In contrast to the pattern of the axial mean velocity distributions, it is found that large turbulence intensities always occur at locations with large velocity gradients. To further explore the turbulence intensity distributions, flows around the block are divided into three regions as follows. (1) In the front region of the block, the axial turbulence intensity has a small value relative to other regions and appears peaks near the upper and lower channel walls. As Y/H<1 (below the centerline), the axial turbulence intensity gradually increases in the streamwise direction owing to obstruction by the block; meantime, its peak level increases. As Y/H>1 (above the centerline), the axial turbulence intensity is minimally influenced by the block, and thus it remains almost unchanged. Conversely, the transverse turbulence intensities are much smaller than the axial intensities in regions before the block. Typically, at X/H=-0.35, the axial peak turbulence intensity is about two times that of the transverse peak turbulence intensity. (2) In the upper region of the block, particularly around the region where the top separating bubble occurs, both the axial and transverse turbulence intensities increase dramatically, an effect of fluid acceleration caused by area contraction. Global maximums of the axial and transverse turbulence intensities occur above the top separating bubble. The cross-sectional peak axial and transverse turbulence intensities first begin to increase in the leading edge station and then decrease until it reaches the trailing edge station. (3) In the rear region of the block, both the axial and transverse peak turbulence intensities gradually increase along the separation line in the streamwise

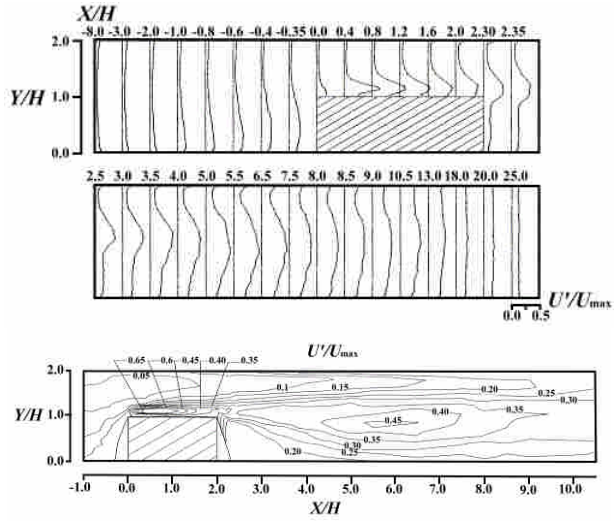

Fig. 10. Axial turbulence intensity and its iso-contour distribution

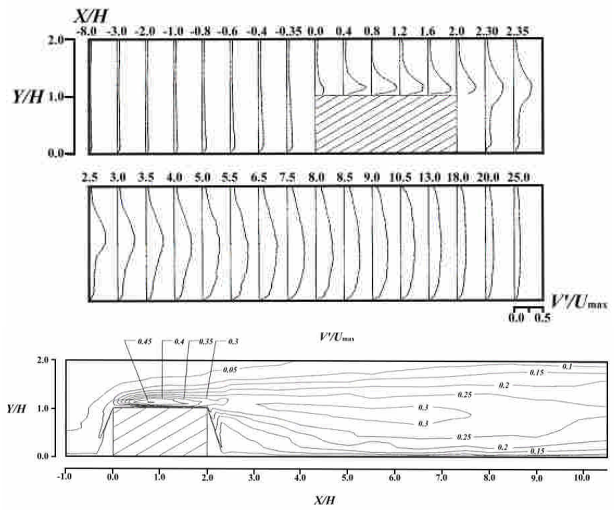

Fig. 11. Transverse turbulence intensity and its iso-contour distributions

direction, and achieve their maximums values at the stations located near 2~3H before the reattachment point, and then gradually decrease until they reach the channel outlet.

In calculations, isotropic and homogeneous conditions are frequently employed to analyze turbulent flows in cases similar to those in this study. These assumptions obviously fail due to the large discrepancy identified between the axial and transverse turbulence intensities. Moreover, the maximal axial turbulence intensity is about 2 times larger than the transverse intensity in the front region of the block, about 1.6 times larger than that in the top region of the block, and 1.8 times larger than that in the rear region of the block.

F. Turbulent kinetic energy

According to Fig. 12, the turbulent kinetic energy has distributions extremely similar to the axial and transverse turbulence intensities throughout the flow. The common characteristics of the fluctuating parameters of *U′*, *V′*, and *K* are summarized as follows.

(1) In the front region of the block, *U′*, *V′*, and *K* all have the lowest values in the centerline of the channel and have two symmetric peak values near the channel walls.

(2) In the upper region of the block, the global maximums of *U′*, *V′*, and *K* appear, indicating the presence of a highly turbulent mixing effect.

(3) In the rear region of the block, the peak values of *U′*, *V′* and *K* all occur near the separation line where large gradient exists. Accordingly, all these fluctuation parameters increase to the second global maximums at stations near 2H~3H before the reattachment point and then decline until they reach the reattachment point. After the reattachment point, they continue to decay and are finally distributed uniformly at the channel outlet.

(4) In the region near the front face of the block and in the near-wall region inside the main separating bubble, *U′*, *V′*, and *K* all have small values relatively to other areas. This phenomenon is attributed to the weak turbulent mixing or fluctuating effect.

The measured distributions of the probability density function (PDF) of the instantaneous velocity indicated that clustering distributions of instantaneous velocity occurred at Y/H=0.03, 0.05, and 0.07 at section X/H=8.5; disperse distributions of instantaneous velocity were found at the intersection of the separation line and section X/H=8.5. This phenomenon confirms the existence of two different flow conditions at the same cross-section, X/H=8.5. Since the reattachment point is the end point on the separation line, a disperse PDF distribution is also expected at this point, i.e., the turbulence intensity at this reattachment point must be as large as any other point on the separation line regardless of the rare

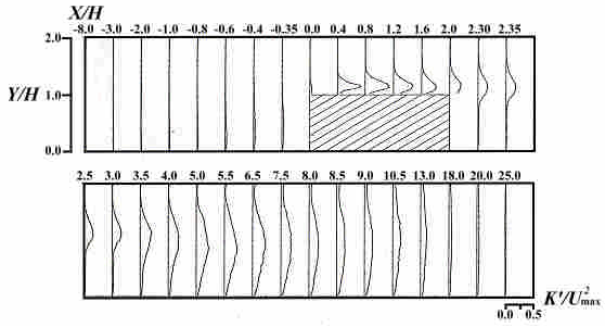

Fig. 12. Turbulent kinetic energy distributions

experimental data taken near this point. Moreover, because the fluid in the area neighboring the reattachment point rushes directly along the separation line onto the reattachment point, it is suggested that high turbulent intensities will appear at this point.

G. Reynolds stress

Turbulent motion is dissipative. To attain energy balance, energy should be continuously imported into the turbulence to maintain its motion. In any turbulent motion, the Reynolds stress plays the role of momentum transfer between different layers. Additionally, the Reynolds stress also dominates the production of turbulence energy. Therefore, the Reynolds stress is a key parameter that governs the turbulent structure. It usually has a large value near the shear layer boundary. This fact can be observed from Boussinesq's eddy-viscosity hypothesis that is frequently used in turbulence modeling:

$$\tau_t = \overline{U'V'} = -\varepsilon \frac{dU}{dy} \qquad (1)$$

This formula implies that high levels of Reynolds stress may happen near the shear-layer boundary where the large velocity gradient happens. To more clearly understand the turbulence structure, the Reynolds stress distribution along the channel was measured. Figure 13 shows that the Reynolds stress is small in the front region of the block relative to other regions in the channel. At the channel inlet, the Reynolds stress is 0 at the centerline owing to the vanishing velocity gradient and has two peaks near the upper and lower channel walls. The occurrence of turbulent boundary layers near the channel walls contributed the formation of these two peaks. Accompanied by the flow approaching the mounted block, the level of Reynolds stress gradually increases. Along the block's top face, the peak Reynolds stress first dramatically increases to its global maximum around station X/H=1.2, then gradually decreases until it meets the trailing edge of the block. Behind the block, the Reynolds stress affected by the separation layer increases again and reaches its second maximum near stations 2~3H before the reattachment point. The Reynolds stress then gradually decreases until it reaches the end of the channel. In the main recirculation region behind the block, the Reynolds stress is relatively small compared with that in other areas in the channel due to the block-obstructing effect. This phenomenon was also indicated in [18] and [22]. Generally, the variations of the peak Reynolds stress throughout the flow are qualitatively the same as those of the peak turbulence intensity and peak turbulent kinetic energy.

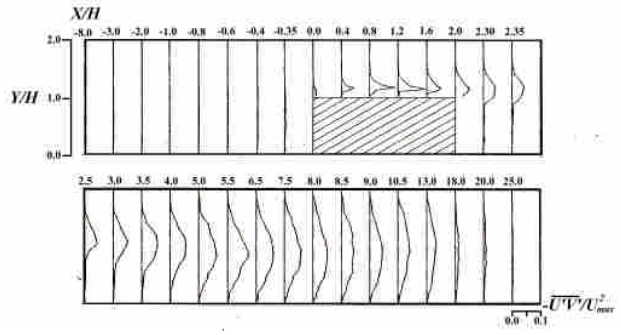

Fig. 13. Reynolds stress distributions

Based on the above results, we concluded that large turbulence intensity, turbulent kinetic energy and even Reynolds stress occur above the block, along the separation line, and near the reattachment point of the main recirculation region. Conversely, low turbulence intensity, turbulent kinetic energy and Reynolds stress occur near the front and the smallest rear circulating bubbles which just attached on the bottom-front and bottom-rear corners of the block, respectively. Eventually, an extremely low heat transfer rate is expected with the development of some hot spots near those separating bubbles. These characteristics are especially evident in the design strategies for cooling systems for electronic equipments.

H. Variations of peak turbulence intensity, kinetic energy, and Reynolds stress

Figure 14 shows the variations of peak axial and transverse turbulence intensities, kinetic energy, and Reynolds stress at Re=11,500 in the top and rear regions of the block. Generally, all peak U', V', K and $-U'V'$, increase dramatically to their global maximums on the block at stations X/H=0.5, 0.5, 0.8, and 1.2, respectively. This phenomenon was attributed to the fluctuating effect caused by passage contraction and flow acceleration. Then, all peak values of U', V', K and $-U'V'$ gradually decrease in the down-stream direction. Along the separation line behind the block, the peak U', V', K and $-U'V'$ gradually rise to their second maximums at stations X*/H=4 and then gradually decline and finally distribute uniformly near the channel outlet.

IV. CONCLUSIONS

This study used the LDV together with the refractive index matching measurement technique to elucidate the turbulence structure of a block-mounted turbulent channel flow and, in particular, in the near-wall recirculation region where traditional measurement instruments fail as a result of ambiguity of the refractive index of the passing laser lights and interference in the flow field. Comprehensive data for U', V',

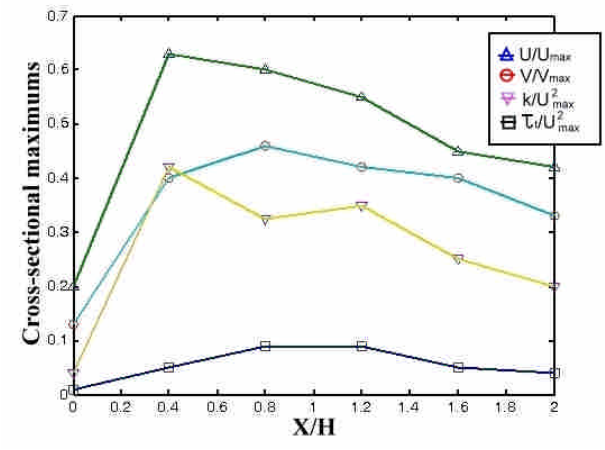

(a) above the block

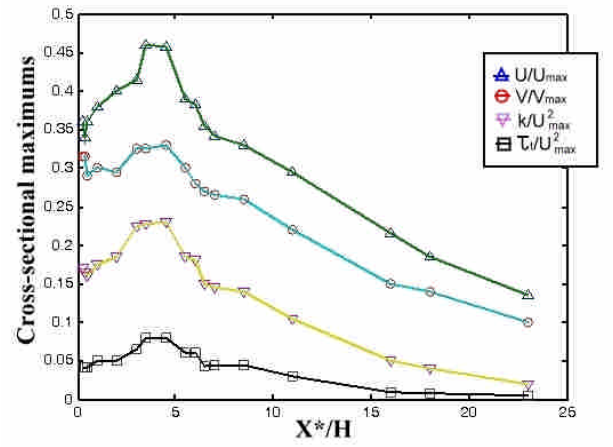

(b) behind the block

Fig. 14. Development of flow parameters

K, $-U'V'$ and C_f distributions were measured throughout the flow and their influence and characteristics were discussed in detail. The experimental results suggest the following conclusions:

(1) Four separating bubbles were identified around the block; one on the bottom-front corner of the block; one on the top face of the block; one on the bottom-rear corner of the block; and the largest behind the block attached to the bottom wall of the channel.

(2) In the rear region of the block, the skin-friction coefficient firstly decreases to its minimum at X^*/X_r=0.4, and then increases monotonously to the main reattachment point (X^*/X_r =1), and finally approaches to a constant value. In the near-wall region of the main recirculation region, the new defined skin-friction coefficient C_{fN} correlates significantly with the shear-layer Reynolds number Re_N. Flows inside the main recirculation region behave similar to the laminar boundary layer flow.

(3) Although axial mean velocity distributions in the main recirculation region behind the block do not adhere to the log-law; but the relation $U^+=Y^+$ still holds for flows sufficiently near the channel wall.

(4) Axial turbulence intensity is much greater than the transverse one around the block. The isotropy assumption which frequently used in most engineering calculations for turbulent channel flows resembling that in this study failed to apply.

(5) Similar distributions along the channel exists for U', V', K, and $-U'V'$. The global maximums of U', V', K, and $-U'V'$ happen on the top face of the block, and their second maximums appear at stations roughly 2~3H before the main reattachment point.

REFERENCES

1. Adams, E. W. and J. P. Johnston (1988) Flow structure in the near-wall zone of a turbulent separated flow. *AIAA Journal*, 26(6), 232-266.
2. Antoniou, J. and G. Bergeles (1988) Development of the reattachment flow behind surface-mounted two-dimensional prism. *ASME Journal of Fluids Engineering*, 110, 127-133.
3. Bergeles, G. and N. Athanassiadis (1983) The flow past a surface-mounted obstacle. *ASME Journal of Fluids Engineering*, 105, 461-463.
4. Buchlin, J. M. (2002) Convective heat transfer in a channel with perforated ribs. *International Journal of Thermal Science*, 41, 332-340.
5. Castro, I. P. and A. Haque (1987) The structure of a turbulent shear layer bounding a separation region. *Journal of Fluid Mechanics*, 179, 439-460.
6. Chen, Y. M. and K. C. Wang (1996) Numerical and experimental studies on laminar forced convective heat transfer in a channel with wurface-mounted heated blocks. *Journal of the Chinese Institute of Engineers*, 19(6), 669-679.
7. Coles, D. (1978) A model for flow in the viscous sublayer. Proceedings of the Workshop on Coherent Structure of Turbulence Boundary Layers, Leihigh Unversity, Bethlehem, 244-263.
8. Driver, D. M. and H. L. Seegmiller (1988) Feature of a reattaching turbulent shear layer in divergent channel flow. *AIAA Journal*, 23(2), 163-198.
9. Durst, F. and A. K. Rastogi (1980) Turbulent flow over two-dimensional fences. *Turbulent Shear Flows*, 2, 218-231.
10. Durst, F., J. Jovanovic and J. Sender (1995) LDA

measurement in the near-wall region of a turbulent pipe flow. *Journal of Fluid Mechanics*, 295, 305-335.

11. Han, J. C., J. S. Park and C. K. Lei (1985) Heat transfer enhancement in channels with turbulence promoters. *ASME Journal of Engineering for Gas Turbines and Power*, 107, 628-643.
12. Jonansson, A. V. and H. P. Alfredsson (1982) On the structure of turbulent channel flow. *Journal of Fluid Mechanics*, 122, 295-325.
13. Jurbran, B. A., S. A. Swiety and M. A. Hamdan (1996) Convective heat transfer and pressure drop characteristics of various array to simulate the cooling of electronic modules. *International Journal of Heat and Mass Transfer*, 39, 3519-3529.
14. Kim, J., P. Moin and R. Moser (1987) Turbulence statistics in a fully developed channel flow at low reynolds number. *Journal of Fluid Mechanics*, 177, 133-166.
15. Liou, T. M. and C. F. Kao (1988) Symmetric and asymmetric turbulent flows in a rectangular duct with a pair of ribs. *ASME Journal of Fluids Engineering*, 110, 373-379.
16. Lyons, S. L., T. J. Hanratty and J. McLaughlin (1991) Large-scale computer simulation of fully developed turbulent channel flow with heat transfer. *International Journal of Numerical Methods in Fluids*, 13, 999-1928.
17. Meinders, E. R. and K. Hanjalic (2002) Experimental study of the convective heat transfer from in-line and staggered configurations of two wall-mounted cubes. *International Journal of Heat Mass Transfer*, 45, 465-482.
18. Myrum, T. A., X. Qiu and S. Acharya (1993) Heat transfer enhancement in a ribbed duct using vortex generators. *International Journal of Heat and Mass Transfer*, 36, 3497-3508.
19. Olsson, C. O. and B. Sundén (1998) Experimental study of flow and heat transfer in rib-roughened rectangular channels. *Experimental Thermal and Fluid Science*, 16(4), 349-365.
20. Patel, V. C., R. Wolfgang and S. Georg (1985) Turbulence models for near-wall and low reynolds number flows: A review. *AIAA Journal*, 23, 1308-1339.
21. Ratts, E., C. H. Amon, B. B. Mikic and A. T. Patera (1988) Cooling enhancement of forced convection air cooled chip array through flow modulation induced vortex shedding cylinders in cross-flow. *Cooling Technology for Electronic Equipment*, 183-194. Hemisphere, New York.
22. Ruderich, R. and H. Fernholz (1986) An experimental investigation of a turbulent shear flow with separation, reverse flow, and reattachment. *Journal of Fluid Mechanics*, 163, 283-311.
23. Simpson, R. L., Y. T. Chew and B. G. Shivaprasad (1981) The structure of a separating turbulent boundary layer. Part 1. Mean flow and Reynolds stress. *Journal of Fluid Mechanics*, 113, 23-45.

Received: Jul. 11, 2005 Revised: Sep. 6, 2005
Accepted: Nov. 7, 2005

NOMENCLATURE

AR aspect ratio ($=W_c/H_c$)

BR blockage ratio ($=H/H_c$)

C_f skin friction coefficient ($=2\tau_w/\rho U_{\max}{}^2$)

C_{fN} skin friction coefficient in the main recirculation region ($=\frac{2\tau_w}{\rho U_N{}^2}$)

H block height, *mm*

H_c channel height, *mm*

K turbulent kinetic energy ($=\frac{3}{4}(U'^2+V'^2)$), $m^2/\sec^2$

L_r reattachment length, *mm*

n refractive index

Re Reynolds number ($=U_{\max}H/\nu$)

Re_N Reynolds number ($=U_N H/\nu$)

U axial mean velocity, *m*/sec

$U_{\max}$ maximal axial mean velocity at station X/H=-8, $m/\sec$

U_N maximal axial mean velocity in the main recirculation region, *m*/sec

U' time-averaged axial turbulence intensity, *m*/sec

U^+ dimensionless axial mean velocity ($=\frac{U}{U^*}$), *m*/sec

U^* friction velocity ($=\sqrt{\frac{|\tau_w|}{\rho}}$), *m*/sec

$-U'V'$ Reynolds stress ($=\varepsilon\frac{dU}{dy}$), $m^2/\sec^2$

V transverse mean velocity, *m*/sec

V' time-averaged transverse turbulence intensity, *m*/sec

W block width, *mm*

W_c channel width, *mm*

X coordinate in the axial direction, originating from the station of the leading edge of the block, *mm*

X_r reattachment length, *mm*

X^* coordinate in the axial direction behind the block (=X-W), originating from the station of the trailing edge of the block, *mm*

Y coordinate in the transverse direction, *mm*

Y^+ dimensionless coordinate in the transverse direction ($=\frac{YU^*}{\nu}$)

Z coordinate in the spanwise direction, *mm*

τ_t Reynolds stress ($=-U'V'$), $m^2/\sec^2$

τ_w wall shear stress($=\mu\frac{\partial U}{\partial Y}\big|_{Y=0}$), N/m^2

ε eddy viscosity, $m^2/\sec$

μ dynamic viscosity, $N\cdot\sec/m^2$

ν kinematic viscosity, $m^2/\sec$

ρ fluid density, kg/m^3